

# Chapter 2

## Complex Behavior of a Buckled Beam Under Combined Harmonic and Random Loading

R. Wiebe and S.M. Spottswood

**Abstract** Nonlinearities have long been avoided in the design of structural systems. This was done to make problems tractable, to fit within current design paradigms, and often with the assumption that the resulting design would be conservative. Computational methods have made the investigation of nonlinear systems possible, which may yield more accurate and optimal designs. However, in venturing into the nonlinear regime, a designer must be aware of potential pitfalls, one of which is the possibility of unsafe responses “hiding in the weeds” of parameter or initial condition space. In this paper, an experimental study on a damped, post-buckled beam in the presence of noise is used to show that co-existing stationary solutions may be present in real-world scenarios. Stochastic resonance, a surprising phenomenon in which a small harmonic load interacts with, and magnifies the response to, an otherwise pure random load, is also studied and observed to occur in the beam.

**Keywords** Nonlinear dynamics • Stochastic resonance • Experimental mechanics • Snap-through • Duffing

### 2.1 Introduction

Co-existing solutions and their basins of attraction are well represented in the literature, however, despite decades of study, even in the simplest case of single-degree-of-freedom (SDOF) models such as the Duffing equation, one may see extremely complex fractal basin of attraction boundaries separating co-existing solutions in initial condition (IC) space [1–3]. An excellent review of the importance, and many of the applications of co-existing solutions in nonlinear dynamics can be found in [4].

Real engineering systems are always subjected to at least some noise, which provides another level of complexity. The response of the Duffing oscillator under noise is studied in [5] for white noise, and [6] for bounded noise under parametric excitation. In nonlinear systems, even when small relative to the random input, harmonic forces may provide a disproportionate amount of energy to the response. This can occur through stochastic resonance. Stochastic resonance typically occurs when the time scale of the mean snap-through rate due to the random loading is close to that of a small harmonic input. The harmonic loading works to alternately deepen and shallow the competing potential wells which, in an average sense, promotes (or makes it more likely that) the response due to the random load will show increased coherence with the harmonic input [7]. As a consequence of this, the harmonic load is also able to do more net work on the system [8]. Good reviews of stochastic resonance, both in two-state and continuous systems, with many other potential applications may be found in the works [9–11].

---

R. Wiebe (✉)

Structural Sciences Center, Air Force Research Laboratory, WPAFB, Dayton, OH 45433, USA

Universal Technology Corporation, Dayton, OH, USA

e-mail: [rwiebe@co.utcd Dayton.com](mailto:rwiebe@co.utcd Dayton.com)

S.M. Spottswood

Structural Sciences Center, Air Force Research Laboratory, WPAFB, Dayton, OH 45433, USA

The studies of stochastic resonance that most closely resemble the work in this paper may be found in [12] and [13, 14]. In the former, a numerical SDOF analogue of a buckled beam is used to investigate the potential for stochastic resonance to improve the performance of vibrational energy harvesters. The latter two include experimental results showing the presence of stochastic resonance in a bi-stable nanomechanical oscillator.

The experimental system studied in this paper is the clamped-clamped post-buckled beam. The nonlinear response of post-buckled beams has been studied for beams subjected to both harmonic loading [15], and random loading [16]. This system presents an ideal avenue for studying nonlinear phenomena in engineering structures as it is an intermediate step in complexity between qualitative discrete models and common structural systems such as curved panels and shells.

## 2.2 The Double-Well Duffing Equation

It is well known that the damped harmonically forced Duffing equation given by  $\ddot{x} + 2\zeta\dot{x} - x + x^3 = A \sin \omega t$  ( $\zeta = 0.05$  in all cases herein) may be used to generate co-existing responses for many different forcing parameters. Several sample time series are shown in Fig. 2.1, where  $P_n$  indicates a response that repeats once every  $n$  forcing cycles. The single-well responses shown in this figure also contain a mirrored twin (not shown) in the other well.

Figure 2.2a shows the Poincaré section of the response,  $x$ , as a function of frequency,  $\omega$ , for a fixed forcing amplitude  $A = 0.3$  in the absence of noise. This plot was obtained by running a simulation at a fixed frequency and plotting the

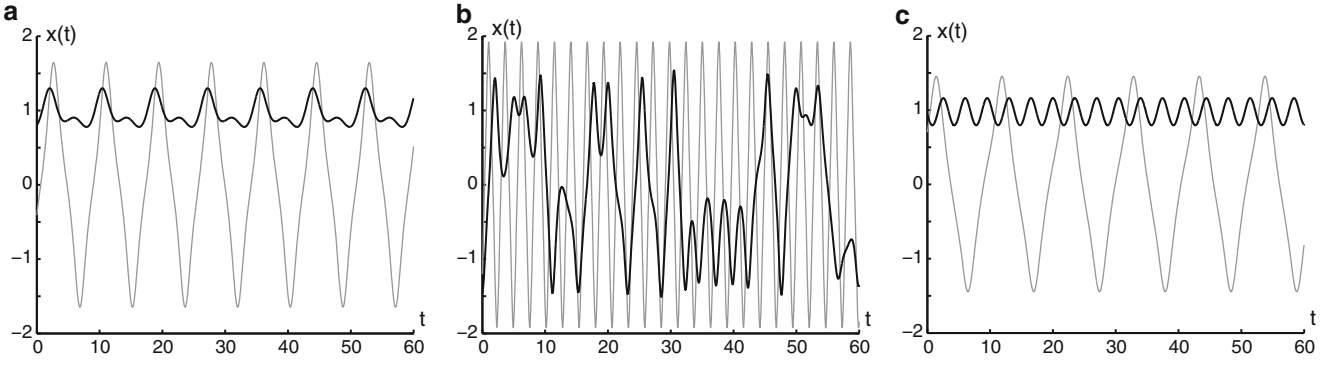


**Fig. 2.1** Sample time series for a damped harmonically forced double-well Duffing oscillator: (a) co-existing  $P_1$  cross-well and single-well responses ( $A = 0.3$ ,  $\omega = 0.75$  rad/s), (b) co-existing cross-well chaos and cross-well  $P_1$  responses ( $A = 0.3$ ,  $\omega = 1.20$  rad/s), and (c) co-existing single-well  $P_1$  and cross-well  $P_3$  responses ( $A = 0.25$ ,  $\omega = 1.80$  rad/s)

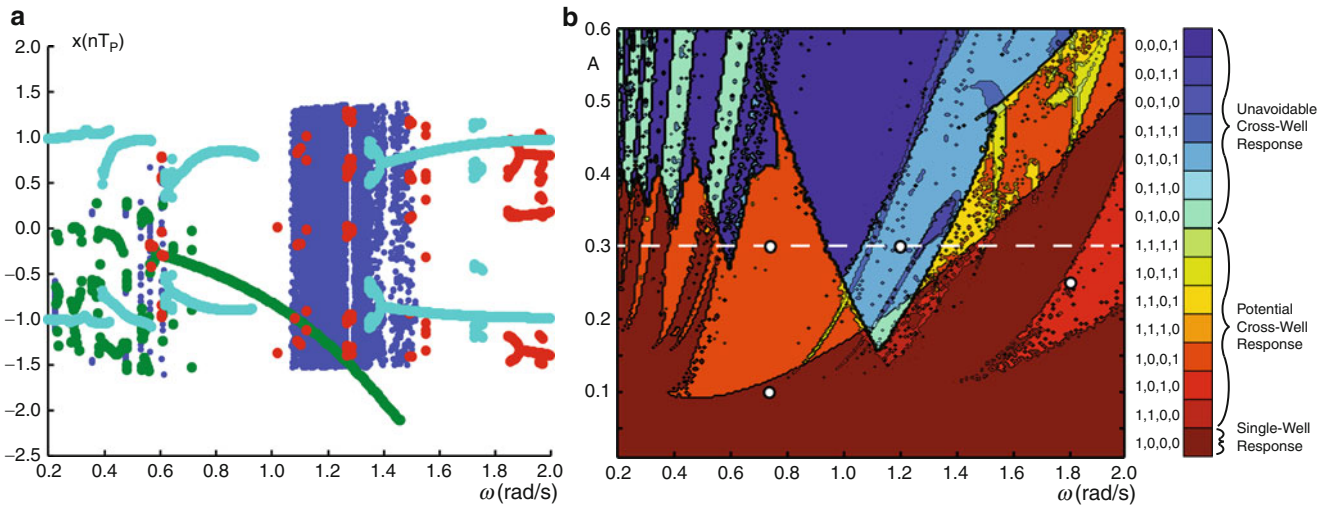


**Fig. 2.2** Co-existing solutions as a function of forcing parameters: (a) A bifurcation diagram in forcing frequency developed using Poincaré sampling at the forcing period. Four types of response are shown; (cyan) Single-well non-chaotic  $P_1$ , (blue) chaotic, (red) cross-well  $P_n$ , (green) cross-well  $P_1$ . (b) Response type chart in forcing parameter space, the four number sequences indicate the existence (1) or non-existence (0) of, in sequence, the cyan, blue, red, and green response types. The horizontal dashed line in part (b) corresponds to the forcing amplitude used in part (a) and the target markers denote forcing parameter pairs of interest (Color figure online)

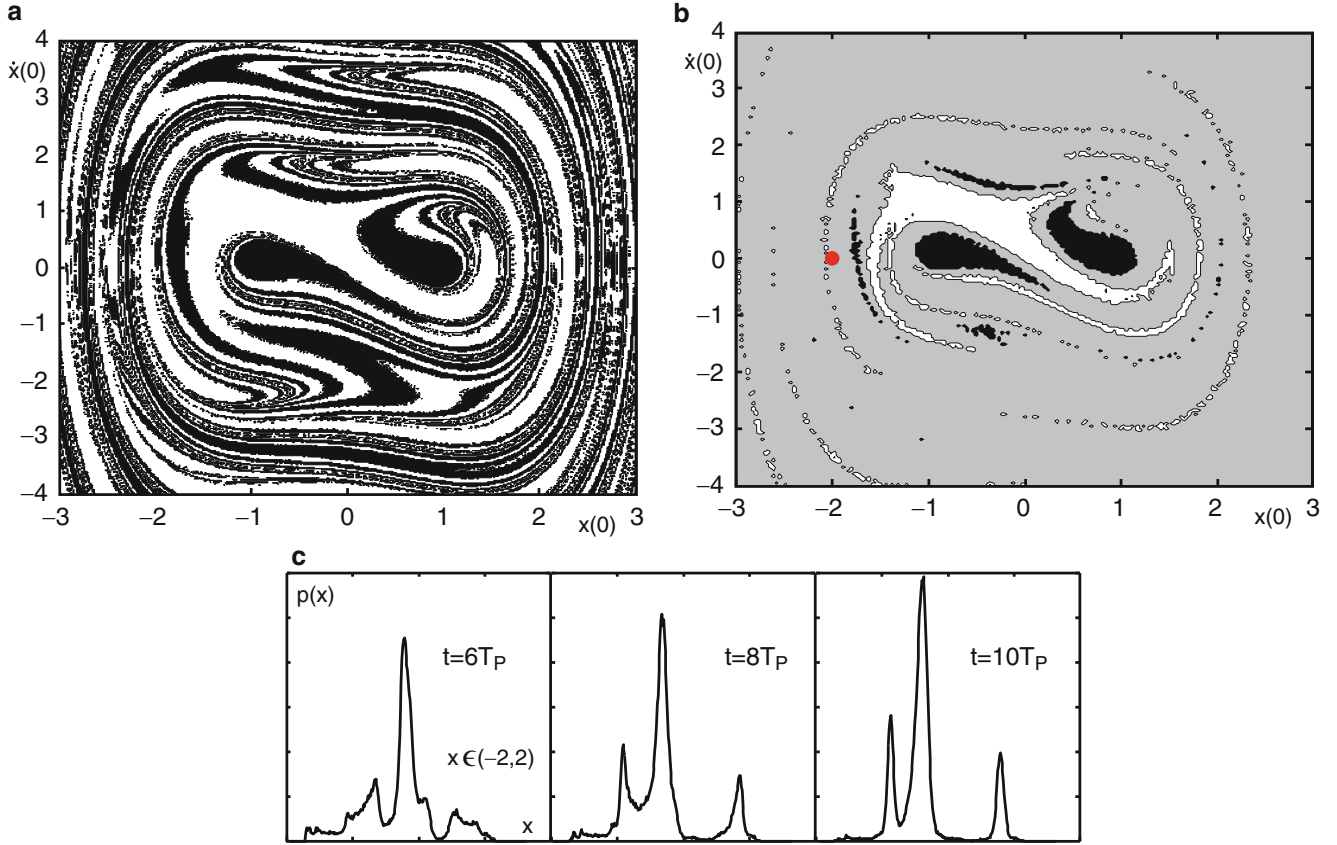


**Fig. 2.3** Basins of attraction under harmonic plus random loading:  $A = 0.3$ ,  $\omega = 0.75$  rad/s for (a)  $\sigma = 0.0$  and (b)  $\sigma = 0.014$ ;  $A = 0.3$ ,  $\omega = 1.20$  rad/s for (c)  $\sigma = 0.0$  and (d)  $\sigma = 0.033$ . White (black) shading indicates ICs inevitably lead to cross-well  $P_1$  (single-well) response in parts (a) and (b) and chaotic (cross-well  $P_1$ ) response in parts (c) and (d). Gray shading indicates ICs which may lead to either type of co-existing response under different realizations of the random forcing process

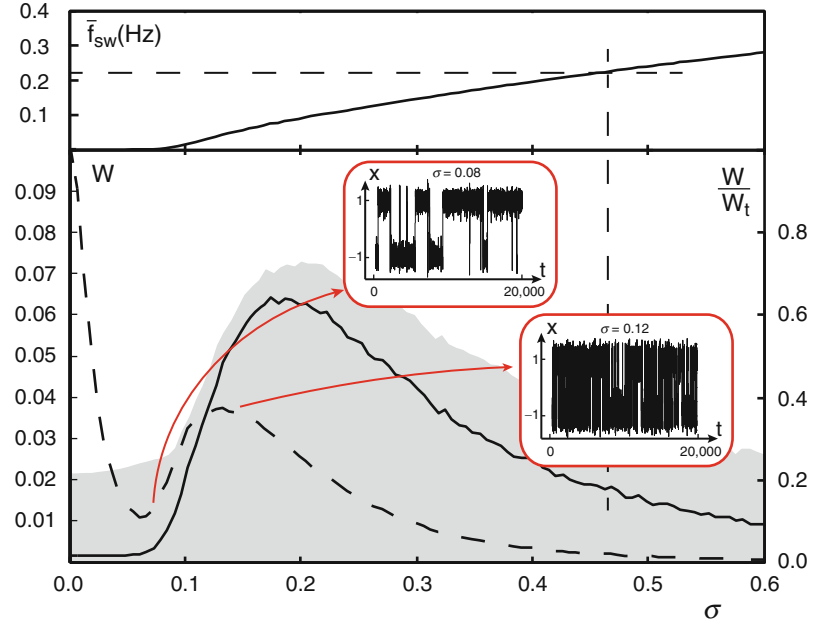
position “ $x$ ” each time the forcing reached a particular phase (after transients were allowed to decay). Hence, in the event of a  $P_n$  response these Poincaré samples repeatedly revisit the same  $n$  points. All of the data points for a particular simulation were color-coded according to the labels in the caption. At each frequency, 60 simulations were performed at random ICs to search for co-existing solutions, which is why many frequencies contain multiple types of color-coded response. The complete procedure was then repeated over a grid of 200 frequencies to yield the final plot. In order to include the effects of all the forcing parameters, in Fig. 2.2b the vertical axis is replaced with the forcing amplitude,  $A$ , (with a resolution of 200) and contours were plotted based on the number and types of responses co-existing at each parameter set. The determination of chaos was done by calculating the sign of the largest Lyapunov exponent ( $\lambda_1$ ) via the method discussed in [17]. The switching (snap-through) frequency, together with the Lyapunov exponent were then used to distinguish between the four types of response in the caption.

The green (cross-well) and cyan (single-well) “paths” of Poincaré points in Fig. 2.2a appear to show more than just a single  $P_1$  response. This may indeed be the case, however, at least one of these is trivial as all responses exist with a  $180^\circ$  phase-lagged mirror image counterpart due to the symmetry of the system.

The level of complexity in Fig. 2.2 is quite surprising considering the simplicity of the equation of motion. The region of potential cross-well response is perhaps of most interest as it is mostly likely to lead to unsafe design in the event where a simulation or experiment, purely by happenstance, only captures the “safe” single-well response. It is therefore of interest whether this region persists under more realistic loading, i.e. in the presence of noise.

A noisy forcing term (a normally distributed random process  $\xi(t) = \sigma u$ , where  $u$  is standard normal) was added to the right-hand-side of the Duffing equation. At low noise levels, the underlying deterministic attractors are not completely destroyed, instead the noise blurs the boundaries in the basins of attraction. This is shown in Fig. 2.3, where the basins of attraction yielding co-existing solutions are shown with and without the addition of the noise term  $\xi(t)$ . The fractal basin boundaries observed in part (a) are a well-known feature of the Duffing system. For part (b), each IC pair was simulated 60 times and in the event that all responses ended up on the same attractor the IC pair was shaded black or white depending

**Fig. 2.4** Stochastic resonance in the Duffing oscillator under combined harmonic plus random forcing at  $A = 0.1$ ,  $\omega = 0.75$  rad/s



on the type of response, however, if each response occurred at least once the IC pair was shaded gray. As the noise level is increased further, eventually the attractors are destroyed completely, at first by occasional jumping between the “ghosts” of the former attractors, and then at really high noise levels the response takes on a new, more random character.

A response of the system in the gray shaded regions of Fig. 2.3b may be better understood by looking at part (c). In this figure the IC denoted by the red dot in part (b) was simulated 100,000 times, the results of which were used to create a time varying probability density plot. At time  $t = 0$  the probability density is a delta function at  $x = -2$ ,  $\dot{x} = 0$ . Only five forcing cycles later it produces a broad density plot. As the time progresses it begins to show three distinct peaks, and after ten forcing cycles it has reached a steady state. Beyond this point, the probability density becomes periodic returning to what is shown once every forcing cycle. It should be noted that the density plots shown are a projection, as the velocity is not shown. The two smaller peaks are in fact the solutions that were trapped in the two potential wells. These two peaks oscillate on either side, while the large peak oscillates across the both wells. After ten forcing cycles the three separate peaks no longer exchange any probability density, and in the full  $x$  and  $\dot{x}$  space they never come in contact. Under higher noise levels intermittency appears as “leakage” between the peaks.

A more complete picture of the response of the Duffing oscillator to increasing noise levels is given in Fig. 2.4 for a grid of 100  $\sigma$  values. The forcing parameters used to develop this plot were in a single-well response region just below potential snap-through (see Fig. 2.2b). This was selected to avoid confusion between stochastic resonance and primarily deterministic cross-well response. The top plot shows the average switching (or snap-through) frequency  $f_{sw}$ , which is the frequency of crossings of the  $x = 0$  hilltop in either direction. The bottom plot in each panel contains the average work caused by the harmonic force component over a single forcing period (solid black curve, left axis), the maximum correlation envelope (shaded gray, left axis), and the ratio of the harmonic to total work (dashed black curve, right axis). Also shown in the insets of this figure is a time series before (showing intermittency) and near stochastic resonance.

The value  $W$  is the average work done by the harmonic component of the total force (through the total displacement) over a single harmonic forcing period and presents a peak value at a nonzero noise level that is much higher than the work under the harmonic load alone. This phenomenon is known as stochastic resonance. Perhaps more meaningful than  $W$ , is the ratio of the average work done by the harmonic force to the total average work  $W_t$  done over a single forcing period. It is not obvious whether, for a given amount of average energy input, if it is better or worse, say in the context of fatigue, that the majority of the energy input be delivered by the harmonic or random force components.

Another interesting result is obtained by plotting the cross-correlation for harmonics at different phases than the true harmonic input (this is no longer work but has the same units). The gray shaded region in Fig. 2.4 shows the envelope of the maximum cross-correlation at each frequency. The phase at which the maximum occurs is potentially different for each point on the envelope. Note that the actual work,  $W$ , can never exceed this envelope, and in this case it in fact does not make any contact.

In the literature it is usually assumed that the resonant peaks in the work  $W$  should occur approximately where the average switching rate is approximately twice (a full response “cycle” requires two switching events) the harmonic forcing frequency ( $f = \omega/2\pi = 0.12$  Hz). The dashed line construction at a frequency equal to twice the harmonic forcing frequency shows that this is not true for this system, although many results in the literature are for heavily overdamped systems.

### 2.3 The Post-Buckled Beam

While useful to come to a phenomenological understanding, it is difficult to determine the relevance of the above results to real world structural systems. In this section, the same types of behavior are shown to occur, both experimentally and using a finite element (FE) model, in a post-buckled beam, which can be seen as an analogue for curved structural systems such as aircraft panels.

The experimental system investigated in this section is a clamped-clamped stainless steel beam as shown in Fig. 2.5 with beam thickness  $t$ , width  $b$ , length  $L$ , modulus of elasticity  $E$ , density  $\rho$ , and coefficient of thermal expansion  $\alpha_T$ . The beam was buckled under various axial loads that were induced by a heat lamp placed several feet in front of the beam (not seen in photograph). The beam was fastened to a shaker which provided harmonic and random loading through base excitation. The power spectral density that was used was a flat band between 50 and 500 Hz with no power at other frequencies.

The various experimental results that follow were also obtained at two temperatures ( $T_1 = 34.7^\circ\text{C}$ ,  $T_2 = 26.1^\circ\text{C}$ ). This was done to promote snap-through at different load levels. The beam was also tested at two different realistic damping levels ( $\zeta_1 = 0.71\%$ ,  $\zeta_2 = 1.70\%$ ) which was adjusted by attaching thin adhesive aluminum constrained layer damping foil strips to the back of the beam. Co-existing responses were quite easy to find at both temperatures and damping levels. The natural frequency of the post-buckled beam at  $T_1$  was found to be 163 Hz.

In order to gain a sense of the robustness of experimental phenomena shown later, and to ensure that they are real physics as opposed to pathological effects of experimental imperfections, the results are compared with those of a numerical model. However, as the focus of this paper is not on developing accurate numerical models, a relatively simple FE approach is taken. Despite the simplicity of the model, the results will be shown to be surprisingly accurate.

The finite element model was developed using the lumped mass co-rotational beam element formulation in [18] with 24 elements, and solved using an arc-length solution following routine. The damping ratios identified experimentally were used to select the coefficient for mass proportional damping. Slightly different temperatures were applied to the FE model ( $T_1 = 35.3^\circ\text{C}$ ,  $T_2 = 27.1^\circ\text{C}$ ) than were observed experimentally. This was done to best match all of experimentally measured static quantities, that being the natural frequencies, temperatures, and the  $y_0$  quantity (distance between the two post-buckled configurations) seen in Fig. 2.5.

As opposed to independently generating harmonic and random loads to match that used in the experiments, the total experimental loading applied to the structure, measured with an accelerometer, was fed into the FE model.

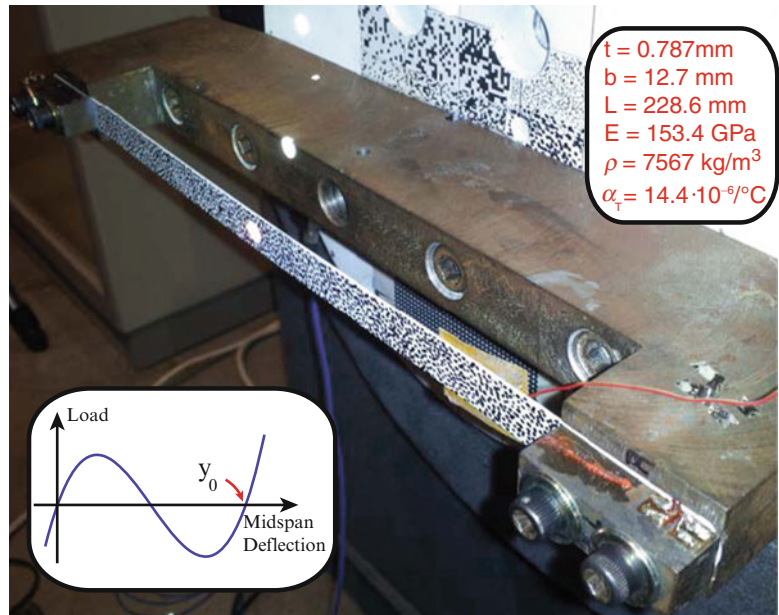


**Fig. 2.5** Photograph of beam clamped to shaker with parameters *inset top right*, and illustrative load-deflection curve under transverse load *inset bottom left*. Damping treatment was applied to the back of the beam



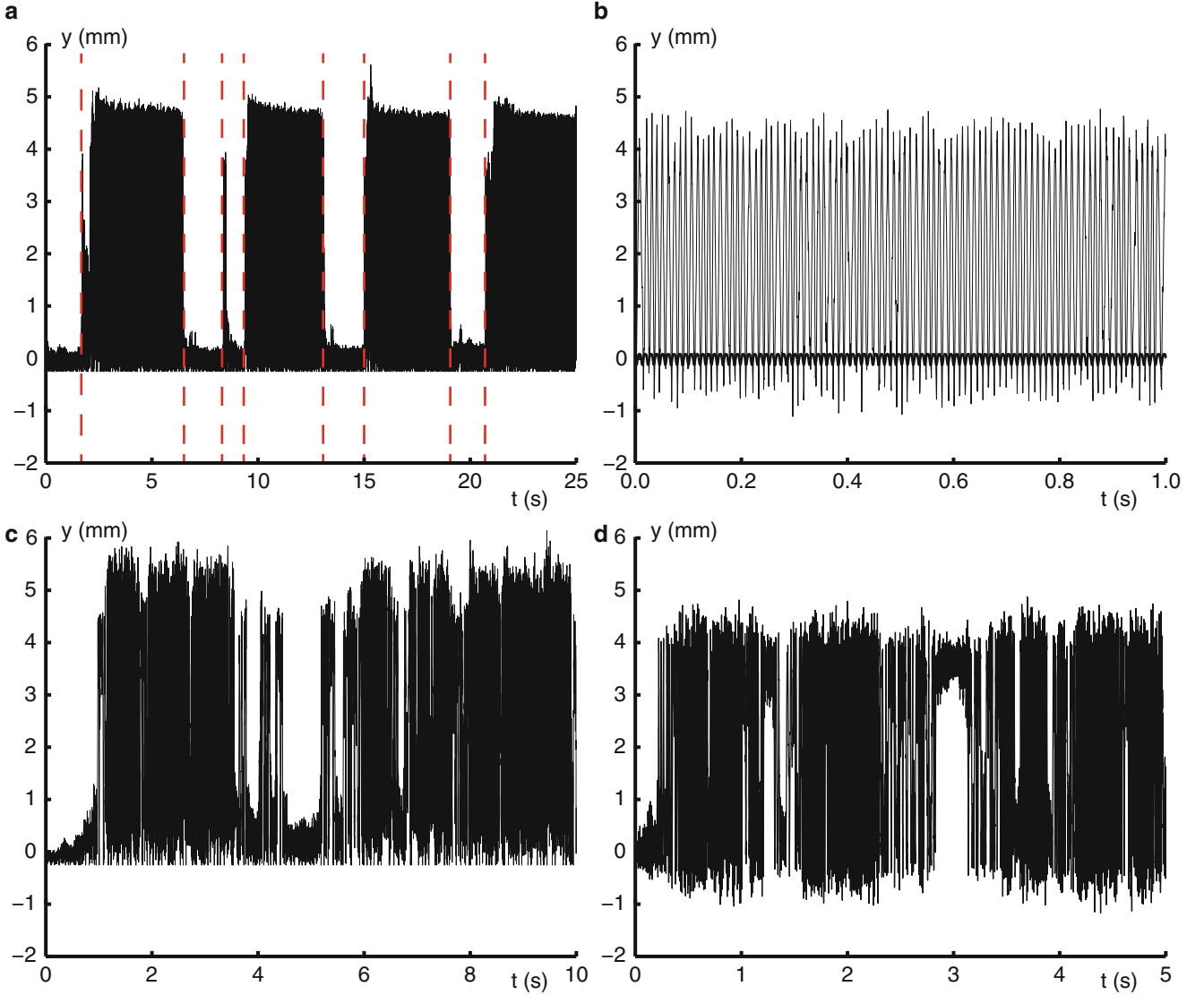


**Fig. 2.6** Affect of increasing noise level on co-existing responses for  $\zeta = \zeta_1$ ,  $T = T_1$ ,  $A = 8.0$  g,  $f = 92$  Hz. (a) Experimental and (b) numerical co-existing responses for  $\sigma = 0.0$  g RMS; (c) experimental and (d) numerical intermittent response for  $\sigma = 3.1$  g RMS. The dashed vertical lines indicate external perturbations

### 2.3.1 Results

The affect of increasing the noise level on the response is illustrated in Fig. 2.6 using forcing parameters which, under pure harmonic loading alone, yielded co-existing snap-through and non-snap-through responses. This was not difficult to find in the system, and could usually be found at almost any thermal load and forcing frequency by varying the forcing amplitude. Parts (a) and (b) show the co-existing experimental and numerical time series under pure harmonic load. The dashed vertical lines in the experimental curves denote external perturbations (a manual disturbance applied to the beam) that were used to search for co-existing solutions. For the numerical plot in part (b) a temporary large amplitude harmonic force was applied to find the snap-through response (light gray curve), while starting from rest yielded the small amplitude response (black). Both the snap-through and non-snap-through responses are periodic, although the snap-through response is slightly less regular. Parts (c) and (d) instead show the response under combined harmonic plus random loading. The response for both systems now appears to intermittently switch between cross-well and single well response. The approximate noise levels at which the co-existing responses in parts (a) and (b) are destroyed in favor of intermittent response was approximately 1.8 g RMS both experimentally and numerically, demonstrating that co-existing response can persist with nontrivial noise intensities. Due to

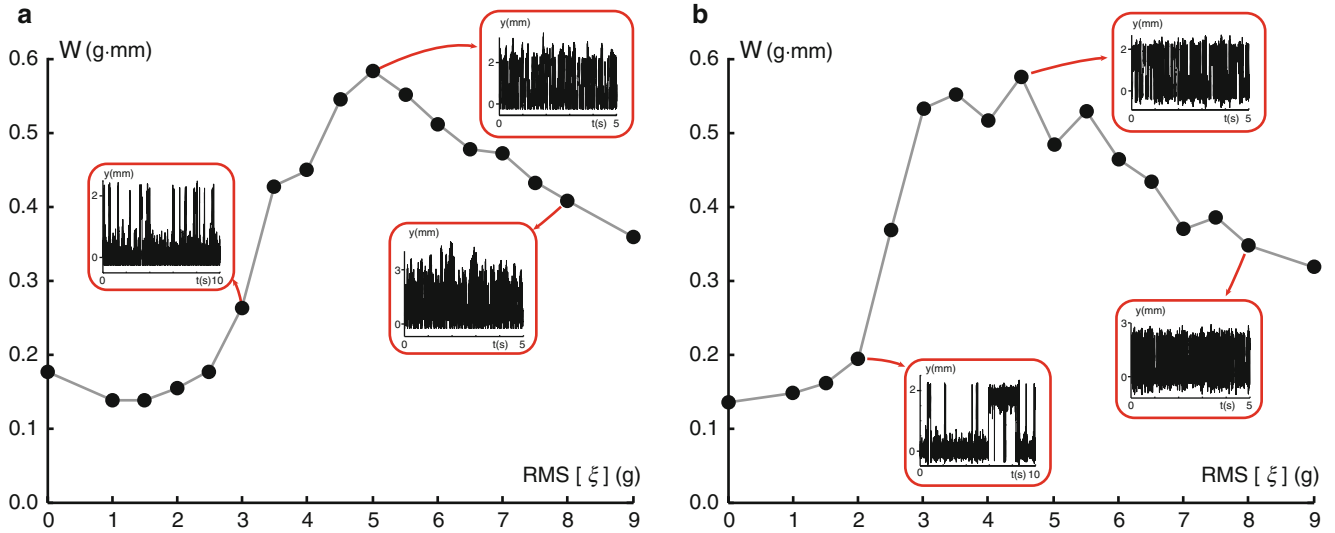


**Fig. 2.7** Stochastic resonance cross-correlation envelope under increasing noise levels (in units of acceleration due to gravity (g)) in post-buckled beam with sample displacement time-series inset: **(a)** experimental, **(b)** numerical.  $\zeta = \zeta_2$ ,  $T = T_2$ ,  $A = 1.0$  g,  $f = 50$  Hz

a DC bias in the laser vibrometer that was used to record the experimental response, the experimental data is all manually shifted to an arbitrary datum. Hence, the absolute value of displacement is not especially meaningful, but the peak-to-peak response is still accurate.

Stochastic resonance was also observed in the buckled beam. Figure 2.7 contains the cross-correlation envelopes for the experimental and numerical response of the structure under increasing noise levels. The harmonic loading parameters used to develop these curves was reduced from 8.0 g down to 1.0 g for practical purposes, as for stochastic resonance it is necessary to apply random loads well in excess of the harmonic load, which was beyond the capability of the shaker for an 8.0 g harmonic load. In order to ensure that cross-well behavior was still accessible under reasonable levels of noise, the temperature of the system was also reduced to  $T = T_2$ .

Stochastic resonance and phase lag are not immediately obvious by visual inspection of time series shown in the insets (also see insets in Fig. 2.4), it must instead be determined by numerically integrating the forces and response over a long time series. Unfortunately, the controller that was used to operate the shaker did not independently report the harmonic and random components of the total input base acceleration. Thus, the work due to the harmonic force cannot be determined. Instead, for each noise level the cross-correlation of the total response velocity was calculated with respect to harmonic functions (with frequency equal to the harmonic forcing frequency) of unit magnitude over a fine grid of 100 initial phase lags. The maximum correlation obtained is the value that is plotted, making this equivalent to the gray shaded envelope in Fig. 2.4 for the Duffing system. The phase at which the maximum correlation occurred has no particular meaning as the time at which the data recording device was turned on was completely random in phase relative to the time when the dynamic loading was initiated.

The correlation envelope is given units of acceleration (since  $A = 1.0$  g) times distance, however, the units are less meaningful than the relative agreement between the experimental and numerical results. Another difference in this plot relative to the results on the Duffing equation is that it is only an approximation of the correlation as only the midspan velocity was recorded. Nonetheless a clear stochastic resonant peak is visible both numerically and experimentally. Each experiment and simulation was based on an 80 s time series (or 4,000 forcing cycles), which was long enough for the averaging routines to reasonably converge without overloading the data acquisition equipment.

## 2.4 Conclusions

The possibility of co-existing responses persisting in the presence of noise and damping, and the phenomenon of stochastic resonance are investigated. Results are shown for both a simple Duffing oscillator, and more importantly, for a post-buckled beam subjected to combined harmonic plus random loading. An FE model is developed to compare with the experimental results of the post-buckled beam with excellent agreement, indicating that these behaviors are not anomalous.

It was observed in this study that co-existing solutions may persist up to nontrivial levels of noise. For more intermediate levels of noise it is shown that intermittency occurs where the system hops between the two formerly stable attractors. Finally, at levels of noise much higher than the harmonic forcing, stochastic resonance was observed. In the vicinity of stochastic resonance the harmonic forcing provides a disproportionate amount of energy to the response. Thus, at all levels of noise, underlying harmonic components continue to greatly affect the response.

**Acknowledgements** The authors wish to thank Tom Eason and Joe Hollkamp for their helpful comments on this work, and Tim Bieborniss and Travis Wyen for their assistance in the laboratory.

## References

1. Pisarchik AN (2001) Controlling the multistability of nonlinear systems with coexisting attractors. *Phys Rev E* 64(4):046203
2. Aguirre J, Sanjuán, MAF (2002) Unpredictable behavior in the duffing oscillator: Wada basins. *Physica D* 171(1):41–51
3. Sommerer JC, Ott E (1996) Intermingled basins of attraction: uncomputability in a simple physical system. *Phys Lett A* 214(5):243–251
4. Feudel U (2008) Complex dynamics in multistable systems. *Int J Bifurcat Chaos* 18(06):1607–1626
5. Dykman MI, Mannella R, McClintock PVE, Moss F, Soskin SM (1988) Spectral density of fluctuations of a double-well duffing oscillator driven by white noise. *Phys Rev A* 37(4):1303
6. Liu WY, Zhu WQ, Huang ZL (2001) Effect of bounded noise on chaotic motion of duffing oscillator under parametric excitation. *Chaos Solitons Fractals* 12(3):527–537
7. Muratov CB, Vanden-Eijnden E, Weinan E (2005) Self-induced stochastic resonance in excitable systems. *Physica D* 210(3):227–240
8. Jung P, Marchesoni F (2011) Energetics of stochastic resonance. *Chaos Interdiscip J Nonlinear Sci* 21(4):047516–047516
9. Gammaitoni L, Hänggi P, Jung P, Marchesoni F (1998) Stochastic resonance. *Rev Mod Phys* 70(1):223
10. Dykman MI, Luchinsky DG, Mannella R, McClintock PVE, Stein ND, Stocks NG (1995) Stochastic resonance in perspective. *Il Nuovo Cimento D* 17(7–8):661–683
11. Wellens T, Shatokhin V, Buchleitner A (2004) Stochastic resonance. *Rep Prog Phys* 67(1):45
12. McInnes CR, Gorman DG, Cartmell MP (2008) Enhanced vibrational energy harvesting using nonlinear stochastic resonance. *J Sound Vib* 318(4):655–662
13. Badzey RL, Mohanty P (2005) Coherent signal amplification in bistable nanomechanical oscillators by stochastic resonance. *Nature* 437(7061):995–998
14. Almog R, Zaitsev S, Shtempluck O, Buks E (2007) Signal amplification in a nanomechanical duffing resonator via stochastic resonance. *Appl Phys Lett* 90(1):013508–013508
15. Poon W-YS (2004) Effect of anti-symmetric mode on dynamic snap-through of curved beam. Ph.D. thesis, The Hong Kong Polytechnic University
16. Gordon RW, Hollkamp JJ, Spottswood SM (2003) Nonlinear response of a clamped-clamped beam to random base excitation. In: *Proceedings of the eighth international conference on recent advances in structural dynamics*, Southampton
17. Xie W-C (2006) *Dynamic stability of structures*. Cambridge University Press, Cambridge
18. Battini J-M (2002) Co-rotational beam elements in instability problems. Ph.D. thesis, KTH



Nonlinear Dynamics, Volume 2

Proceedings of the 32nd IMAC, A Conference and  
Exposition on Structural Dynamics, 2014

Kerschen, G. (Ed.)

2014, VIII, 319 p. 256 illus., 208 illus. in color.,

Hardcover

ISBN: 978-3-319-04521-4